NeuroImage: Clinical 36 (2022) 103199

Contents lists available at ScienceDirect

NeuroImage: Clinical

journal homepage: www.elsevier.com/locate/ynicl

Selective atrophy of the cervical enlargement in whole spinal cord MRI of amyotrophic lateral sclerosis

Robert L. Barry [a,b,c,*], Angel Torrado-Carvajal [a,d], John E. Kirsch [a,b], Grae E. Arabasz [a], Daniel S. Albrecht [a], Zeynab Alshelh [a], Olivia Pijanowski [e], Austin J. Lewis [e], Mackenzie Keegan [e], Beverly Reynolds [e], Paulina C. Knight [e], Erin J. Morrissey [a], Marco L. Loggia [a,b,f], Nazem Atassi [e,g,h], Jacob M. Hooker [a,b,1], Suma Babu [e,g,*,1]

[a] *Athinoula A. Martinos Center for Biomedical Imaging, Department of Radiology, Massachusetts General Hospital, Charlestown, MA, USA*
[b] *Department of Radiology, Harvard Medical School, Boston, MA, USA*
[c] *Harvard–Massachusetts Institute of Technology Health Sciences & Technology, Cambridge, MA, USA*
[d] *Medical Image Analysis and Biometry Laboratory, Universidad Rey Juan Carlos, Madrid, Spain*
[e] *Sean M. Healey & AMG Center for ALS at Massachusetts General Hospital, Department of Neurology, Neurological Clinical Research Institute, Boston, MA, USA*
[f] *Department of Anesthesia, Critical Care and Pain Medicine, Massachusetts General Hospital, Boston, MA, USA*
[g] *Department of Neurology, Harvard Medical School, Boston, MA, USA*
[h] *Sanofi Genzyme, Cambridge, MA, USA*

ARTICLE INFO

Keywords:
Atrophy
Cross-sectional area
Cervical enlargement
Spinal cord
Magnetic resonance imaging
Amyotrophic lateral sclerosis

ABSTRACT

Amyotrophic lateral sclerosis (ALS) is a deadly neurodegenerative disorder affecting motor neurons in the spinal cord and brain. Studies have reported on atrophy within segments of the cervical cord, but we are not aware of previous investigations of the whole spinal cord. Herein we present our findings from a 3T MRI study involving 32 subjects (15 ALS participants and 17 healthy controls) characterizing cross-sectional area along the entire cord. We report atrophy of the cervical enlargement in ALS participants, but no evidence of atrophy of the thoracolumbar enlargement. These results suggest that MR-based analyses of the cervical cord may be sufficient for *in vivo* investigations of spinal cord atrophy in ALS, and that atrophy of the cervical enlargement (C4–C7) is a potential imaging marker for quantifying lower motor neuron degradation.

1. Introduction

Amyotrophic lateral sclerosis (ALS) is a neurodegenerative disorder affecting motor neurons in the spinal cord and brain that leads to rapidly progressive loss of limb and bulbar muscle function, and, ultimately, respiratory failure and death within 3–5 years. Human *in vivo* neuroimaging has shown focal areas of cortical atrophy in the vicinity of upper motor neurons in the brains of people with ALS (Alshikho et al., 2016). However, brain findings focus only on the upper motor neuron component of ALS pathology. *In vivo* imaging of the spinal cord and lower motor neuron (LMN) component remains challenging due to the small diameter of the cord and need for high spatial resolution coupled with unavoidable motion artifacts from physiological motion such as respiration, cardiac activity and cerebrospinal fluid (CSF) pulsatility (El Mendili et al., 2019). The literature on spinal cord imaging in ALS continues to emerge, but remains sparse with variable study designs, data acquisitions (including field strength and pulse sequences), and/or outcome metrics (cross sectional area, volume, fractional anisotropy, etc.), which have resulted in varying and often inconsistent findings across studies (El Mendili et al., 2019).

Advances in *in vivo* spinal cord imaging technologies and methods may offer opportunities to mitigate some of the aforementioned challenges (Bede et al., 2012; Bede et al., 2018; El Mendili et al., 2019). Previous 1.5T (Agosta et al., 2009) or 3T (Cohen-Adad et al., 2013; Querin et al., 2017; Paquin et al., 2018; van der Burgh et al., 2019) studies have demonstrated spinal cord atrophy and/or diffusion abnormalities affecting the cervical cord in ALS participants. One study (Paquin et al., 2018) reported that cervical gray matter atrophy was more sensitive than spinal cord atrophy to discriminate participants with ALS. However, spinal cord neuroimaging studies have mostly

* Corresponding authors.
E-mail addresses: Robert.Barry@mgh.Harvard.edu (R.L. Barry), sbabu@mgh.Harvard.edu (S. Babu).
[1] These authors share senior authorship.

https://doi.org/10.1016/j.nicl.2022.103199
Received 31 March 2022; Received in revised form 26 August 2022; Accepted 13 September 2022
Available online 16 September 2022

focused on cervical cord MRI findings – and often just segments of the cervical cord. To the best of our knowledge, *no studies to date have reported on the feasibility and challenges of high-resolution MRI along the entire spinal cord in people with ALS*. Therefore, the goal of the current study was to evaluate the spatial distribution of atrophy along the entire spinal cord in ALS participants compared to healthy controls. A secondary objective subserving this aim was the development of appropriate MRI sequences for whole cord measurements of cross-sectional area.

2. Material and methods

2.1. Study cohort

As outlined in the Consort diagram (Fig. 1), 54 subjects were prescreened/screened and 46 subjects were enrolled in this study. Thirty-two subjects (15 participants with ALS and 17 healthy controls) completed this study between July 2016 and March 2021. All subjects met the institutional PET/MRI safety criteria (including being able to lie supine for approximately two hours) and provided written, informed consent through protocols approved by the Mass General Brigham (formerly Partners HealthCare) Institutional Review Board (IRB) and Radioactive Drug Research Committee.

Cohort characteristics are detailed in Table 1. Our ALS cohort is enriched by participants with arm dysfunction and with relatively preserved leg function. Notably, nearly two-thirds of the ALS cohort had arm onset ALS while all ALS participants included in the final analyses showed upper limb weakness and muscle atrophy at the time of scan. At the time of scan, nearly one-third of ALS participants ($n = 4$) had intact leg/gross motor function as measured by the ALSFRS-R subdomain score (12 out of 12), while nearly one-third ($n = 4$) had severe arm weakness as measured by an ALSFRS-R fine motor subscore of ≤ 4 out of 12. The ALS and healthy control (HC) groups were similar for age, sex, race, and ethnicity. All ALS participants underwent cervical-thoracolumbar spinal cord MRI scans. To expand the sample size and minimize sampling bias, the HC cohort included 7 subjects from a separate project led by a co-author (M.L.L.) that acquired thoracolumbar MRI scans in the same scanner with the same acquisition parameters. Exclusion criteria for HCs were similar across projects.

All ALS participants were diagnosed as having suspected, possible, probable, probable laboratory-supported, or definite ALS, according to the revised El Escorial criteria. Participants with a history of untreated depression or other psychiatric illnesses, other neuroinflammatory or neurodegenerative diseases, chronic infections, or prior spine surgery were excluded from the study. Genetic testing was not performed as part of the study and clinical genetic testing results were not available/collected for most ALS participants at the time of their participation. While our ALS cohort was of a reasonable sample size, an even larger cohort with genetic testing results would have been required to conduct

Table 1
Group characteristics for MRI cross-sectional area analyses. There are no significant differences in age ($p = 0.085$), sex ($p = 0.137$), race ($p = 0.165$), or ethnicity ($p = 1.0$) between groups. ALSFRS-R slope = [(baseline_ALSFRS-R – 48)/ disease_duration].

Characteristic	ALS ($n = 15$) %(n)/ $\mu(\sigma)$	Controls ($n = 17$) %(n)/ $\mu(\sigma)$
Age at screening (yrs)	53.5 (7.8)	46.4 (14.0)
Sex	male 73% (11)	male 47% (8)
Race	Caucasian 93% (14)	Caucasian 88% (15)
	Native Hawaiian or other Pacific Islander 7% (1)	Black 12% (2)
Ethnicity	not Hispanic or Latino 100% (15)	not Hispanic or Latino 100% (17)
Genetic abnormality	C9orf72 positive (1) SOD1 (Leu145Ser pathogenic variant) (1) TBK1 positive (1) unknown (12)	n/a
Onset region	arm 60% (9) leg 20% (3) bulbar 20% (3)	n/a
Symptom onset to diagnosis (months)	13.2 (8.0)	n/a
Disease duration at scan (months)	32.4 (15.8)	n/a
Revised El Escorial criteria	definite (4) probable (3) probable lab-supported (4) possible (2) suspected (2)	n/a
Spinal segment with LMN dysfunction at scan	arm 100% (15) leg 53% (8) bulbar 0% (0)	n/a
ALSFRS-R total score at scan	34.5 (6.4)	n/a
Estimated ALSFRS-R slope (points/ month)	–0.46 (0.19)	n/a
ALSFRS-R fine motor subdomain score at scan (range = 0–12)	6.3 (3.2)	n/a
ALSFRS-R gross motor subdomain score at scan (range = 0–12)	7.8 (3.2)	n/a
Slow vital capacity at scan (% predicted)	84.5 (15.1)	n/a
Riluzole use at scan	80% (12)	n/a

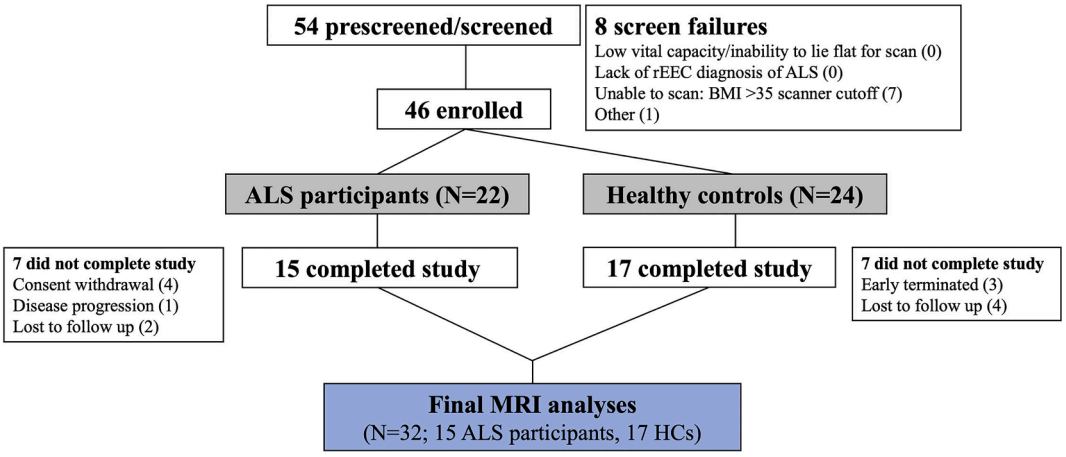

Fig. 1. Consort diagram for MRI data analyses. (rEEC = revised El Escorial criteria).

clinical correlations with MRI data and report meaningful clinical relevance; therefore, clinical correlations are not reported herein.

2.2. Data acquisition

Eligible subjects underwent a combined [^{11}C]PBR28-PET/MRI scan at the Athinoula A. Martinos Center for Biomedical Imaging, Massachusetts General Hospital (Charlestown, MA), performed with a Siemens Biograph mMR whole-body 3 Tesla PET/MR system (Siemens Healthineers, Erlangen, Germany) (Delso et al., 2011). Complete details of the spinal cord PET experiment will be presented in a separate report.

High-resolution T2-weighted MRI scans were acquired to compute spinal cord cross-sectional area (CSA), which is critical for accurate anatomical definition and segmentation of the spinal cord from surrounding cerebrospinal fluid and nerve root contrasts. After an interim analysis and quality control (QC) assessment of MRI data, unanticipated technical challenges were discovered that affected cervical spinal cord data in some scans, attributed to small cord volumes coupled with motion artifacts arising from sialorrhea (i.e., excessive salivation), repetitive swallowing, and effortful breathing that are not uncommon to ALS disease populations. As a result, we improved our MRI acquisition protocol and workflow to mitigate partial volume effects and the impact of deleterious sources of physiological noise while being mindful of the acquisition times to reduce participant discomfort. The revised and finalized cervical cord protocol used a 3D T2-SPACE (Sampling Perfection with Application-optimized Contrasts by using flip angle Evolution) sequence (Chokshi et al., 2017) and consisted of the following parameters: FOV $= 268 \times 358$ mm, matrix size $= 288 \times 384$, sagittal orientation, number of slices $= 64$, in-plane encoding resolution $= 0.93$ mm $\times$ 0.93 mm, slice thickness $= 0.9$ mm, voxel volume $= 0.78$ mm^3, phase encode direction $=$ A–P, phase oversampling $= 25\%$, slice oversampling $= 25\%$, TR $= 1500$ ms, TE $= 103$ ms, RESTORE (i.e., driven equilibrium) magnetization, constant refocusing flip angle $= 120^\circ$, concatenations $= 1.4$, GRAPPA acceleration factor $= 3$, readout flow compensation, sampling bandwidth $= 723$ Hz/pixel, echo spacing $= 5.83$ ms, echo train duration $= 268$ ms, turbo factor $= 59$, acquisition time $= 5$ min 33 s. The original scan parameters (not shown) resulted in an 8 min 24 s acquisition time (due in part to an H–F phase encode direction) vs. a revised time of 5 min 33 s using the above parameters, which improved ALS participants' ability to tolerate lying still for the scan while maintaining high signal-to-noise ratio (SNR) and data quality. Nonetheless, to account for potential ALS participant motion during at least one anatomical scan, the T2-weighted cervical scan was repeated for each subject and the highest quality scan (through a visual inspection by R.L.B.) was included in final analyses.

Thoracolumbar images for all subjects were acquired using a 2D T2-weighted turbo spin echo (TSE) sequence with the following protocol parameters: FOV $= 232 \times 240$ mm, matrix size $= 269 \times 384$, sagittal orientation, number of slices $= 30$, slice gap $= 25\%$, in-plane encoding resolution $= 0.86$ mm $\times$ 0.63 mm, slice thickness $= 2.0$ mm, voxel volume $= 1.08$ mm^3, phase encode direction $=$ H–F, phase oversampling $= 100\%$, TR $= 3380$ ms, TE $= 109$ ms, RESTORE (i.e., driven equilibrium) magnetization, refocusing flip angle $= 150^\circ$, concatenations $= 2.0$, readout flow compensation, sampling bandwidth $= 228$ Hz/pixel, echo spacing $= 10.9$ ms, turbo factor $= 17$, acquisition time $= 7$ min 7 s. Both high-resolution scans were performed with the respective anatomy of interest (cervical or thoracolumbar cord) approximately centered at the scanner isocenter.

2.3. Data processing and analysis

Data were processed and analyzed using in–house code written in MATLAB (MathWorks, Natick, MA) with functions from the Spinal Cord Toolbox (development version, pre-v5.3.0, downloaded March 19, 2021) (De Leener et al., 2017). First, all MR images were resampled (`sct_resample`) to 0.7-mm isotropic resolution as recommended by the developers because the acquired data were anisotropic (personal correspondence; (Gros et al., 2019)). Second, to ensure accurate registration to template space, points were manually labeled (`sct_label_utils`) at the C2/C3 and C7/T1 intervertebral discs, respectively, for cervical images. Similarly, for thoracolumbar images, points were manually labeled at the extents of the spinal cord that were within the imaging field of view (typically T6/T7 or T7/T8, and T12/L1 or L1/L2, respectively). Third, the spinal cord was automatically segmented from the image (`sct_deepseg_sc`). Fourth, the MR image was warped (`sct_warp_template`) to the PAM50 spinal cord and brainstem template (De Leener et al., 2018). Fifth, measurements of cross-sectional area were extracted for each vertebral level (`sct_process_segmentation`). While the entire cervical spinal cord was visualized in all subjects, an imaging gap in the mid-thoracic cord (e.g., Fig. 2) was present in some, but not all, subjects. Because the primary MRI outcome was mean CSA *per vertebral level* (Fig. 3), CSA measurements of vertebral levels with partial coverage were treated in the same way as levels with complete coverage. In a few subjects, the cervicothoracic and thoracolumbar segments overlapped slightly; in such cases, CSA was calculated using each segment, and the greater value was taken as the final CSA to compensate for the downward bias in CSA measurement in low SNR regions.

Group-level comparisons for mean spinal cord CSA across vertebral levels C1 to L1 were performed using one-tailed Wilcoxon rank sum tests with the *a priori* hypothesis that ALS $<$ Control. If a vertebral level for a given subject contained no CSA measurement, then the statistical test between groups was performed with the remaining data. Because contiguous tests along the cord are not statistically independent, Bonferroni correction with a correction factor of 3 was used to correct for multiple comparisons considering that the spinal cord has three distinct anatomical segments (cervical, thoracic, and lumbar).

Investigating group-level changes in spinal cord CSA as a function of vertebral level creates a spatial sensitivity bias because the length of the cord varies across subjects (De Leener et al., 2018). Specifically, we expect lower sensitivity more caudally due to the variability in overlap of the thoracolumbar enlargement (see Fig. 7 in (De Leener et al., 2018)), which is a potential confound in our investigation of whole cord atrophy. We addressed this issue through a secondary analysis of the CSA data where, for each subject, vertebral level C1 was used as an "anchor point" and CSA measurements were linearly scaled so that the thoracolumbar enlargement and cauda equina approximately aligned across subjects prior to group-level averaging. Statistical comparisons for mean spinal cord CSA at each point along the cord between C1 and the cauda equina were then performed as previously described for vertebral levels.

3. Results

Fig. 3 presents the mean CSA across vertebral levels for the entire spinal cord with group-level comparisons between HCs ($n = 17$) and ALS participants ($n = 15$) at each level. Across ALS participants, spinal cord atrophy was not uniform and predominantly presented in the cervical cord compared to other cord segments. Upon review of the vertebral levels within the cervical cord, reductions in CSA were significant at C4, C5, C6, and C7 vertebral level cord segments ($p < 0.05$ or $p < 0.01$; corrected for multiple comparisons), indicating flattening of the characteristic cervical cord enlargement. The CSA $\mu(\sigma)$ in mm^2 for HCs and ALS participants, respectively, at these four cervical levels are: 71.3 (9.29) vs. 60.4 (7.60) at C4, a 15.3% decrease ($p = 0.019$); 71.0 (7.72) vs. 58.7 (8.91) at C5, a 17.3% decrease ($p = 0.009$); 64.6 (6.89) vs. 55.2 (8.51) at C6, a 14.6% decrease ($p = 0.020$); and 56.6 (7.39) vs. 48.2 (8.92) at C7, a 15.1% decrease ($p = 0.049$). Interestingly, there was no evidence of atrophy in the ALS cohort at the level of the thoracolumbar enlargement.

Fig. 4 plots group-level CSA analyses following the rescaling procedure aligning the thoracolumbar enlargement and cauda equina of

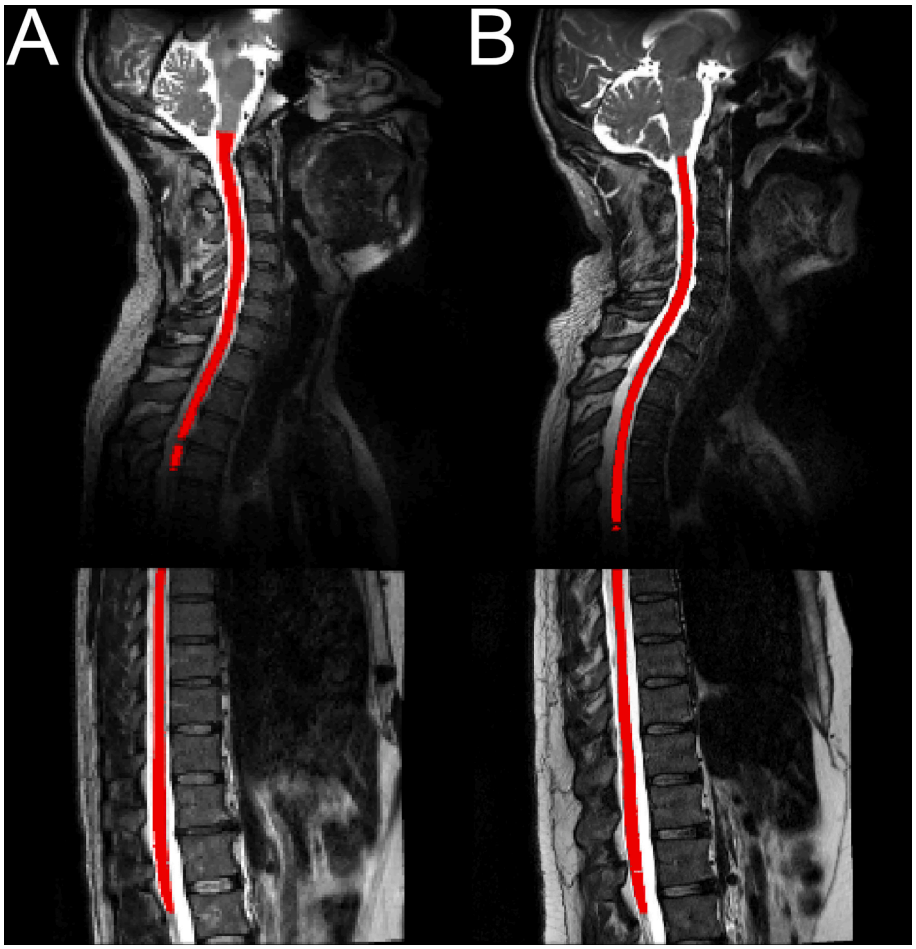

Fig. 2. Mid-sagittal view of the cervicothoracic and thoracolumbar spinal cord segments in (**A**) a healthy control and (**B**) an ALS participant. The spinal cord, automatically identified using the Spinal Cord Toolbox (De Leener et al., 2017), is overlaid in red. The mid-thoracic cord, especially T4–T7, is challenging to image across subjects with two segments due to its distance from the head/neck coil array and the field of view and positioning of the thoracolumbar segment (details of how this is handled are described in the Methods). Atrophy of the cervical cord is visible in this ALS participant.

individual spinal cords to mitigate decreased sensitivity to CSA differences in caudal regions. It is important to note that both cervicothoracic and thoracolumbar cord segments have comparable high imaging data quality, which were QCed by a clinically-blinded investigator during analyses (R.L.B.). No group differences were observed at the thoracolumbar enlargement following normalization, while statistically significant group-level differences were still observed at the cervical enlargement region.

4. Discussion

The spinal cord is a critical region of the central nervous system involved in ALS disease biology affecting LMNs and descending corticospinal tracts. Despite this, there is sparse evidence about regional distribution patterns and *in vivo* changes of atrophy and other mechanistic alterations affecting the spinal cord in human ALS. Two recent 3T studies reported cervical cord atrophy in ALS participants, but these studies evaluated limited portions of the cervical spinal cord (Grolez et al., 2018; Wimmer et al., 2020). The Grolez *et al.* study (Grolez et al., 2018) evaluated a short segment of the cord between vertebral levels C3 and C5 in 40 ALS participants and observed correlations of spinal cord volume reduction with slow vital capacity decline from baseline. Another recent multi-center study ($N = 103$) similarly examined only the rostral cervical cord (C1–C3) and observed a 5% decrease in cord CSA at these levels in ALS compared to HCs at baseline (60.8 mm^2 vs. 63.8 mm^2) (Wimmer et al., 2020).

To the best of our knowledge, the whole cord investigation presented herein is the first to report on non-uniform atrophy and selective degeneration of the cervical cord enlargement in ALS. Across all spinal cord segments, significant atrophy was observed only between vertebral levels C4 to C7, inclusive, in the ALS cohort. Interestingly, there was no evidence of atrophy in the thoracic cord or thoracolumbar enlargement (between vertebral levels T11 and L1) in our ALS participants – even after the rescaling procedure to align the thoracolumbar enlargement and cauda equina of individual spinal cords prior to group analyses. Therefore, *selective atrophy of the cervical enlargement (C4–C7) is a potential imaging marker for quantifying LMN degeneration in ALS*.

An additional contribution of this study was the development of an improved MRI protocol for reliable measurements of spinal cord morphometry. In developing an MRI biomarker for spinal cord neurodegeneration tracking and prediction modeling in ALS, defining the spinal cord/CSF margins accurately is fundamental for accurate cord segmentation. Our 3D T2-SPACE protocol for high-resolution MRI of the upper spinal cord covers the entire cervical cord and upper thoracic cord in a reasonable scan time that permits accurate delineation of the cord boundaries. Additionally, we repeat this scan and allow for the selection of the best acquisitions in case one of the volumes is compromised due to motion from swallowing or head movements, etc., which is not uncommon in the ALS population. Thus, this cervical cord imaging technique with a repeat acquisition could be important in guiding a high-yielding spinal cord MRI session for quantifying LMN degeneration in ALS that could have direct clinical impact in the future.

It is known from studies of fresh, non-fixed spinal cord from non-ALS cadavers (Ko et al., 2004; Watson et al., 2009) and *in vivo* spinal cord MRI of HCs (Frostell et al., 2016; De Leener et al., 2018) that CSA increases from C1 to vertebral levels C4–C5 (*spinal* levels C5–C6) and then decreases in the upper thoracic segments. Our HC data follow this physiological pattern of CSA change along the cord length and show

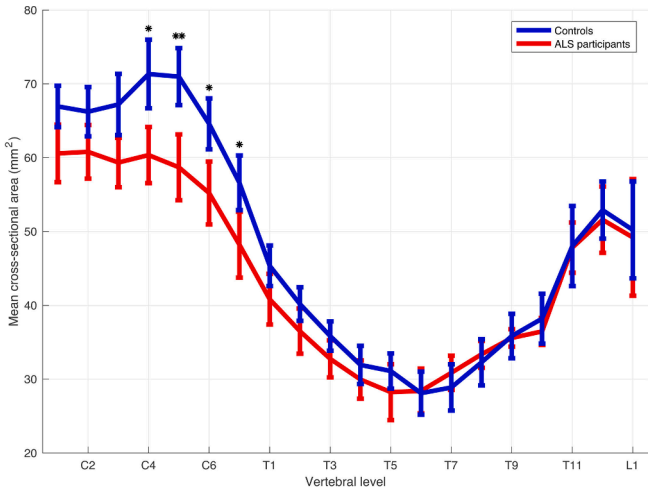

	C4	C5	C6	C7
Controls CSA $\mu(\sigma)$ (mm^2)	71.3 (9.29)	71.0 (7.72)	64.6 (6.89)	56.6 (7.39)
ALS CSA $\mu(\sigma)$ (mm^2)	60.4 (7.60)	58.7 (8.91)	55.2 (8.51)	48.2 (8.92)
% difference (p-value)	−15.3% (0.019)	−17.3% (0.009)	−14.6% (0.020)	−15.1% (0.049)

Fig. 3. Whole spinal cord cross-sectional area (CSA) in healthy controls (n = 17; blue) and ALS participants (n = 15; red) across vertebral levels. Intervertebral discs were used to register individual spinal cords to the PAM50 template for analyses and comparisons. Lines represent mean and standard deviation across subjects within each cohort. Group-level differences between controls and ALS participants are observed across vertebral levels C4 to C7 (* = $p < 0.05$; ** = $p < 0.01$; corrected for multiple comparisons), demonstrating atrophy of the cervical enlargement but preservation of the thoracolumbar enlargement (between vertebral levels T11 and L1) in ALS participants. The primary finding – significant group-level differences in CSA at these four cervical levels – is, for convenience, also summarized in tabular form.

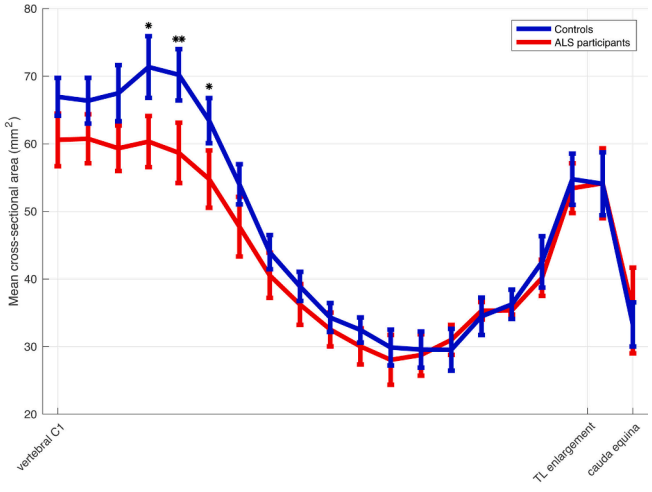

Fig. 4. Whole spinal cord cross-sectional area (CSA) in healthy controls (n = 17; blue) and ALS participants (n = 15; red) following a rescaling procedure (described in the Methods) to align the thoracolumbar (TL) enlargement and cauda equina across subjects to mitigate decreased sensitivity to CSA changes in caudal regions. Lines represent mean and standard deviation across subjects within each cohort. No group-level differences are observed at the thoracolumbar enlargement while statistically-significant differences are still observed at the cervical enlargement (* = $p < 0.05$; ** = $p < 0.01$; corrected for multiple comparisons).

cervical enlargement as expected at vertebral levels C4–C5. Furthermore, the numerical values for CSA in our HC cohort are in good agreement with the PAM50 spinal cord atlas for all levels (De Leener et al., 2018), thus providing additional validation of the representativeness of this study's HC cohort and that CSA values and patterns of atrophy observed in the ALS cohort reflect true biological changes.

One reason for the selective involvement of the cervical enlargement could be related to the universal presence of arm weakness clinical phenotype in our ALS study cohort. In our cohort, all participants had arm weakness while only half experienced leg weakness at the time of scan. Another reason may be the hypothesized selective motor neuron vulnerability in the cervical enlargement region, which is supported by clinical and electrodiagnostic studies showing non-contiguous and preferential limb muscle involvement in ALS (Babu et al., 2017; Shayya et al., 2018; Nijssen et al., 2017). It has been hypothesized that regional differences in motor neuron density, metabolic energy demands, glial activation abnormalities, etc., may explain preferential lower motor neuron vulnerability in different cord regions (Nijssen et al., 2017). For example, a seminal ALS postmortem study revealed widespread pTDP-43 pathology across the entire spinal cord, with the heaviest neuronal loss correlating strongly with the distribution of TDP-43 pathology most prominently at spinal levels C5–T1 and L5 (with corresponding vertebral levels C4–C7 and T12–L1, respectively) (Brettschneider et al., 2014).

The spinal cord MRI findings from this study support future longitudinal quantitative MRI (qMRI) studies in larger, clinically-homogeneous ALS cohorts. Such larger cohort studies must focus on stratifying and enriching subgroups based on phenotypic homogeneity such as leg, arm, truncal, or bulbar weakness at the time of scan to better evaluate other cord regions with confidence. Specifically, the cervical enlargement (C4–C7) is a potential high-yielding region for qMRI in ALS. Future ALS studies could focus on this specific region of interest to increase the likelihood of detecting cord atrophy while reducing scan time and patient discomfort, which should improve scan tolerability and thus recruitment/retention for longitudinal qMRI studies. While designing future clinical association studies using cervical spinal cord qMRI, it is important to recognize that the cervical enlargement is a complex anatomical system showing somatotopic arrangement of motor neurons in both transverse and longitudinal patterns. Even though the origin of a motor unit innervating a certain muscle/myotome is defined by the vertebral level from which it arises (e.g., intrinsic hand muscles by C8–T1 nerve roots), the spinal cord segment within each vertebral level is complex and motor neurons innervating C8–T1 myotomes may be distributed both transversely and longitudinally across multiple adjacent vertebral levels (Watson et al., 2009). Regardless, the focused approach of evaluating the widest segment of the spinal cord – the cervical enlargement – would accelerate further development and scaling of spinal cord qMRI for clinical disease tracking and overall prediction of upper limb functional decline in ALS.

CRediT authorship contribution statement

Robert L. Barry: Funding acquisition, Conceptualization, Data curation, Formal analysis, Investigation, Methodology, Project administration, Software, Validation, Visualization, Writing - original draft, Writing - review & editing. **Angel Torrado-Carvajal:** Investigation, Writing - review & editing. **John E. Kirsch:** Investigation, Methodology, Writing - review & editing. **Grae E. Arabasz:** Investigation, Writing - review & editing. **Daniel S. Albrecht:** Investigation, Writing - review & editing. **Zeynab Alshelh:** Investigation, Writing - review & editing. **Olivia Pijanowski:** Investigation, Writing - review & editing. **Austin J. Lewis:** Investigation, Writing - review & editing. **Mackenzie Keegan:** Investigation, Writing - review & editing. **Beverly Reynolds:** Investigation, Writing - review & editing. **Paulina C. Knight:** Investigation, Writing - review & editing. **Erin J. Morrissey:** Investigation, Writing - review & editing. **Marco L. Loggia:** Funding acquisition, Conceptualization, Data curation, Formal analysis, Investigation, Methodology,

Project administration, Supervision, Validation, Writing - review & editing. **Nazem Atassi:** Funding acquisition, Conceptualization, Investigation, Methodology, Project administration, Supervision, Writing - review & editing. **Jacob M. Hooker:** Funding acquisition, Conceptualization, Formal analysis, Investigation, Methodology, Project administration, Validation, Writing - review & editing. **Suma Babu:** Funding acquisition, Conceptualization, Data curation, Formal analysis, Investigation, Methodology, Project administration, Supervision, Validation, Visualization, Writing - original draft, Writing - review & editing.

Declaration of Competing Interest

In the past two years, J.M.H. has consulted for Amathus Therapeutics, Rodin Therapeutics, Abata Therapeutics, FogPharma, Sanofi-Aventis, Longitude Capital, and the Alzheimer's Drug Discovery Foundation. J.M.H. is a paid Editor-in-Chief for ACS Chemical Neuroscience. J.M.H. is a co-founder and equity holder in Eikonizo Therapeutics (a license holder to J.M.H. patents) and in Sensorium Therapeutics. J.M.H. is a scientific advisory board member and equity holder in Psy Therapeutics, Delix Therapeutics, and Fuzionaire Diagnostics. J.M.H. has received sponsored research grants from Atai Life Sciences and Expesicor and has received honoraria for speaking or advisory service at non-profit academic institutions. N.A. is currently employed by Sanofi Genzyme. The other authors declare that they have no known competing financial interests or personal relationships that could have appeared to influence the work reported in this paper.

Acknowledgments

The authors acknowledge the generosity of our participants and their families. We also thank Dr. Sabrina Paganoni, Paul Cernasov, Catherine Cebulla, and Ning Liu for assistance with subject recruitment and/or protocol management, and Dr. Julien Cohen-Adad for helpful discussions on data preprocessing using the Spinal Cord Toolbox. Imaging was performed at the Massachusetts General Hospital (MGH) Athinoula A. Martinos Center for Biomedical Imaging using resources provided by the Center for Functional Neuroimaging Technologies (P41EB015896) and the Center for Mesoscale Mapping (P41EB030006), Biotechnology Resource Grants supported by the National Institute of Biomedical Imaging and Bioengineering, National Institutes of Health (NIH). The NIH also provided support through grants R01NS094306 and R01NS095937 (M.L.L.), and R01EB027779 (R.L.B.). This research was also supported in part by the MGH Research Scholars Program (J.M.H.), the American Association of Neuromuscular & Electrodiagnostic Medicine Foundation, the American Academy of Neurology Richard Olney Clinician Scientist Development Award in ALS (S.B.), ALS Finding A Cure (N.A.), and the MGH Athinoula A. Martinos Center for Biomedical Imaging. The content is solely the responsibility of the authors and does not necessarily represent the official views of the NIH.

References

Alshikho, M.J., Zürcher, N.R., Loggia, M.L., Cernasov, P., Chonde, D.B., Izquierdo Garcia, D., et al., 2016. Glial activation colocalizes with structural abnormalities in amyotrophic lateral sclerosis. Neurology 87, 2554–2561.

El Mendili, M.M., Querin, G., Bede, P., Pradat, P.F., 2019. Spinal cord imaging in amyotrophic lateral sclerosis: historical concepts – novel techniques. Front Neurol. 10, 350.

Bede, P., Bokde, A.L.W., Byrne, S., Elamin, M., Fagan, A.J., Hardiman, O., 2012. Spinal cord markers in ALS: diagnostic and biomarker considerations. Amyotroph. Lateral Scler. 13, 407–415.

Bede, P., Querin, G., Pradat, P.F., 2018. The changing landscape of motor neuron disease imaging: the transition from descriptive studies to precision clinical tools. Curr. Opin. Neurol. 31, 431–438.

Agosta, F., Rocca, M.A., Valsasina, P., Sala, S., Caputo, D., Perini, M., et al., 2009. A longitudinal diffusion tensor MRI study of the cervical cord and brain in amyotrophic lateral sclerosis patients. J. Neurol. Neurosurg. Psychiatry 80, 53–55.

Cohen-Adad, J., El Mendili, M.M., Morizot-Koutlidis, R., Lehéricy, S., Meininger, V., Blancho, S., et al., 2013. Involvement of spinal sensory pathway in ALS and specificity of cord atrophy to lower motor neuron degeneration. Amyotroph. Lateral Scler. Frontotemporal Degener. 14, 30–38.

Querin, G., El Mendili, M.M., Lenglet, T., Delphine, S., Marchand-Pauvert, V., Benali, H., et al., 2017. Spinal cord multi-parametric magnetic resonance imaging for survival prediction in amyotrophic lateral sclerosis. Eur. J. Neurol. 24, 1040–1046.

Paquin, M.Ê., El Mendili, M.M., Gros, C., Dupont, S.M., Cohen-Adad, J., Pradat, P.F., 2018. Spinal cord gray matter atrophy in amyotrophic lateral sclerosis. AJNR Am. J. Neuroradiol. 39, 184–192.

van der Burgh, H.K., Westeneng, H.J., Meier, J.M., van Es, M.A., Veldink, J.H., Hendrikse, J., et al., 2019. Cross-sectional and longitudinal assessment of the upper cervical spinal cord in motor neuron disease. Neuroimage Clin. 24, 101984.

Delso, G., Fürst, S., Jakoby, B., Ladebeck, R., Ganter, C., Nekolla, S.G., et al., 2011. Performance measurements of the Siemens mMR integrated whole-body PET/MR scanner. J. Nucl. Med. 52, 1914–1922.

Chokshi, F.H., Sadigh, G., Carpenter, W., Allen, J.W., 2017. Diagnostic quality of 3D T2-SPACE compared with T2-FSE in the evaluation of cervical spine MRI anatomy. AJNR Am. J. Neuroradiol. 38, 846–850.

De Leener, B., Lévy, S., Dupont, S.M., Fonov, V.S., Stikov, N., Collins, D.L., et al., 2017. SCT: Spinal Cord Toolbox, an open-source software for processing spinal cord MRI data. Neuroimage 145, 24–43.

Gros, C., De Leener, B., Badji, A., Maranzano, J., Eden, D., Dupont, S.M., et al., 2019. Automatic segmentation of the spinal cord and intramedullary multiple sclerosis lesions with convolutional neural networks. Neuroimage 184, 901–915.

De Leener, B., Fonov, V.S., Collins, D.L., Callot, V., Stikov, N., Cohen-Adad, J., 2018. PAM50: unbiased multimodal template of the brainstem and spinal cord aligned with the ICBM152 space. Neuroimage 165, 170–179.

Grolez, G., Kyheng, M., Lopes, R., Moreau, C., Timmerman, K., Auger, F., et al., 2018. MRI of the cervical spinal cord predicts respiratory dysfunction in ALS. Sci. Rep. 8, 1828.

Wimmer, T., Schreiber, F., Hensiek, N., Garz, C., Kaufmann, J., Machts, J., et al., 2020. The upper cervical spinal cord in ALS assessed by cross-sectional and longitudinal 3T MRI. Sci. Rep. 10, 1783.

Ko, H.Y., Park, J.H., Shin, Y.B., Baek, S.Y., 2004. Gross quantitative measurements of spinal cord segments in human. Spinal Cord 42, 35–40.

Watson, C., Paxinos, G., Kayalioglu, G., 2009. The spinal cord: a Christopher and Dana Reeve Foundation text and atlas. Academic Press.

Frostell, A., Hakim, R., Thelin, E.P., Mattsson, P., Svensson, M., 2016. A review of the segmental diameter of the healthy human spinal cord. Front Neurol. 7:238.

Babu, S., Pioro, E.P., Li, J., Li, Y., 2017. Optimizing muscle selection for electromyography in amyotrophic lateral sclerosis. Muscle Nerve 56, 36–44.

Shayya, L., Babu, S., Pioro, E.P., Li, J., Li, Y., 2018. Distal predominance of electrodiagnostic abnormalities in early-stage amyotrophic lateral sclerosis. Muscle Nerve 58, 389–395.

Nijssen, J., Comley, L.H., Hedlund, E., 2017. Motor neuron vulnerability and resistance in amyotrophic lateral sclerosis. Acta Neuropathol. 133, 863–885.

Brettschneider, J., Arai, K., Del Tredici, K., Toledo, J.B., Robinson, J.L., Lee, E.B., et al., 2014. TDP-43 pathology and neuronal loss in amyotrophic lateral sclerosis spinal cord. Acta Neuropathol. 128, 423–437.